COMPDYN 2011
III ECCOMAS Thematic Conference on
Computational Methods in Structural Dynamics and Earthquake Engineering
M. Papadrakakis, M. Fragiadakis, V. Plevris (eds.)
Corfu, Greece, 25–28 May 2011

INTEGRATION OF GEOMETRY AND FINITE ELEMENTS IN THE ANALYSIS OF NONLINEAR SYSTEMS

Ahmed A. Shabana[1], **Ashraf M. Hamed**[1], **Paramsothy Jayakumar**[2], **and Michael D. Letherwood**[2]

[1] Department of Mechanical and Industrial Engineering
University of Illinois at Chicago
842 West Taylor Street
Chicago, Illinois 60607, U.S.A.
e-mail: {shabana, aabdal5}@uic.edu

[2] U.S. Army RDECOM-TARDEC
6501 E. 11 Mile Road
Warren, MI 48397-5000, U.S.A.
e-mail: {paramsothy.jayakumar, mike.letherwood}@ us.army.mil

Keywords: Geometric discontinuities; Finite element; Multibody systems; B-spline; NURBS.

Abstract. *In this paper, a method for the **i**ntegration of **c**omputer **a**ided **d**esign and **a**nalysis (I-CAD-A) is discussed. The method is based on using a finite element formulation that employs a kinematic description that is consistent with computational geometry methods. This allows for the development of an efficient interface between CAD systems and finite element (FE) and multibody system (MBS) software using simple linear coordinate transformation. The finite element absolute nodal coordinate formulation (ANCF) is used to successfully achieve this integration. ANCF structural finite elements, such as beams, plates, and shells, define shapes that are invariant under arbitrary rigid body displacements. It is shown in this paper that B-spline geometry can always be converted to ANCF geometry. The converse, however, is not true. ANCF provides the flexibility of selecting the basis functions, allowing for the development of finite elements with less number of degrees of freedom as compared to the B-spline counterparts. It is also demonstrated that the B-spline representation fails to capture certain type of discontinuities. To this end, C^0 discontinuities are classified as structural and non-structural discontinuities. Structural discontinuities do not allow for rigid body displacement between the finite elements, while non-structural discontinuities allow for such a rigid body displacement. Using ANCF finite elements, new FE/MBS meshes can be developed. These new FE meshes allow for describing mechanical joints that permit relative rigid body rotations using linear connectivity conditions. Furthermore, the new FE meshes have constant mass matrix and zero Coriolis and centrifugal forces despite the large relative rotation between the finite elements of the structure. Numerical results are presented in order to demonstrate the integration of CAD and FE/MBS analysis.*

1 INTRODUCTION

The geometry description used in many of the existing finite element (FE) formulations cannot be exactly converted to the geometry developed by computational geometry methods such as B-spline and NURBS (**N**on-**U**niform **R**ational **B**-**S**plines) representations. This fact has motivated researchers in the mechanics community to adopt the methods of computational geometry as analysis tools instead of using conventional FE formulations. While the methods of computational geometry, such as B-spline, have several desirable analysis features; these methods have serious limitations when used as analysis tools. The B-spline recurrence formula and the rigid definition of the knot vector make B-spline less attractive as compared to the *absolute nodal coordinate formulation* (ANCF) geometry description. While B-spline geometry can always be converted exactly to ANCF geometry [1-3], the converse is not always true. ANCF geometry does not restrict the order of the parameters or the number of basis functions used in the interpolating polynomials [4-14]. This advantage, as will be demonstrated in this paper, allows for developing finite elements with less number of degrees of freedom as compared to those developed using the B-spline geometry. Another fundamental difference between B-spline and ANCF geometric descriptions lies in modeling discontinuities. There are two types of discontinuities when chain systems are considered [15]. The first is *structural discontinuity* which does not allow rigid body displacement between two elements connected at the joint definition point. This joint allows only for deformation degrees of freedom. The second type of discontinuity is called *non-structural discontinuity* which allows for rigid body displacement at the joint definition point. Figure 1 shows a chain which has a structural discontinuity at point C and non-structural discontinuity at point O. At the junction at C, only deformation degrees of freedom are allowed, while at point O, relative rigid body rotation is permitted. Nonetheless, the degree of continuity at both points is C^0. B-spline can be used as an analysis tool to describe the non-structural C^0 discontinuity at point O, but because of its rigid recurrence structure and the definition of its knot vector and knot multiplicity, B-spline cannot be used in the motion analysis of structural C^0 continuity at point C since B-spline C^0 description leads to a rigid body mode; that is, the elimination of one control point by reducing the knot multiplicity by one is not sufficient for eliminating the modes of rigid body rotations between two B-spline segments. ANCF geometry, on the other hand, can be used in the analysis of both structural and non-structural discontinuities [15].

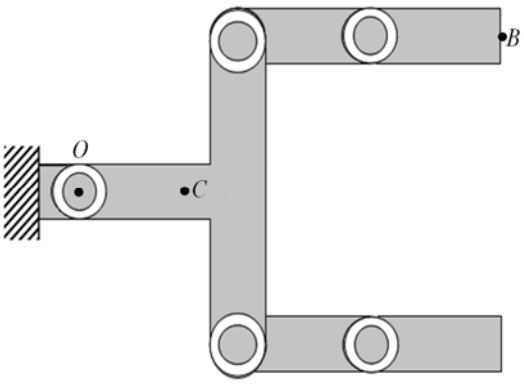

Figure 1 System with structural and non-structural discontinuities

Example of *Non-structural discontinuities* that characterize the motion of MBS applications is chain of links connected by pin joints as the one shown in Fig. 2. Each link is permitted to undergo an independent rigid body rotation. If the links are considered to be flexible bodies, the relative motion between the links is a combination of rigid body and deformation displacements. Nonetheless, the dynamics of a simple planar rigid-link chain is governed by highly nonlinear equations as the result of the geometric nonlinearities due to the finite relative rotations. Existing FE algorithms and computer programs, however, do not allow for generating a FE mesh for such chains using linear connectivity conditions. One of the main goals of this investigation is to develop a new three-dimensional flexible-link chain model using fully parameterized ANCF finite elements. This chain model is based on a new FE mesh defined using linear connectivity conditions. The FE mesh allows for relative rigid body rotations between its elements and has a constant inertia matrix and zero Coriolis and centrifugal forces. In order to develop the new flexible-link chain model presented in this paper, a new pin joint model is introduced. At the joint definition point, different degrees of continuity are used with different parameters; leading to some strain components to be continuous while the others are discontinuous. The modes of deformation at the joint definition points are discussed in order to shed light on the nature of the new joint and kinematic constraints developed in this paper.

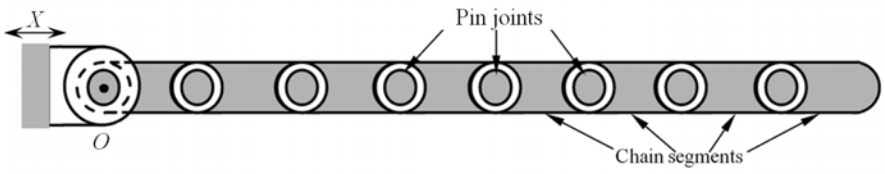

Figure 2 Eight-link chain system

The second main contribution of this paper is to demonstrate the fundamental differences between B-spline and ANCF geometries. It is shown that while B-spline geometry can always be converted to ANCF geometry, the converse is not true because of the rigid B-spline recurrence structure. It is also shown that B-spline representation can be used only in the analysis of one type of C^0 continuity; while such a B-spline representation cannot be used in the analysis of another type of C^0 continuity referred to as structural discontinuity. It is shown that ANCF finite elements which have degrees of freedom less than their B-spline counterparts can be developed since ANCF does not have specific requirements on the order of the parameterization variables or the number of basis functions used in the interpolating polynomials.

2 CONSTRAINT NONLINEARITIES

Existing FE algorithms and computer codes allow for developing meshes in which the finite elements are rigidly connected. In the case of arbitrarily large relative rigid body rotations between the finite elements of one mesh, an incremental solution procedure based on a corotational formulation is used. This FE solution procedure leads to a highly nonlinear inertia matrix and due to the nature of the incremental approach used and the set of coordinates employed, existing FE algorithms and computer programs are not suited for the analysis of complex multibody systems that are characterized by geometric nonlinearities that result from the independent rigid body rotations of the finite elements. In most formulations, including rigid

body dynamics formulations, such non-structural geometric discontinuities are governed by nonlinear algebraic constraint equations which lead to highly nonlinear inertia matrix. For such articulated systems, components which are not rigidly connected are treated as separate bodies when MBS algorithms are used. Consider, for example, the simple planar double-pendulum example shown in Fig. 3. The pendulum consists of two rigid bodies, i and j, connected by a pin (revolute) joint at point P whose local position vector is defined in the two body coordinate systems by the vectors $\bar{\mathbf{u}}_P^i$ and $\bar{\mathbf{u}}_P^j$, respectively. The global position vector of this point in terms of the coordinates of bodies i and j are denoted as $\mathbf{r}_P^i$ and $\mathbf{r}_P^j$, respectively.

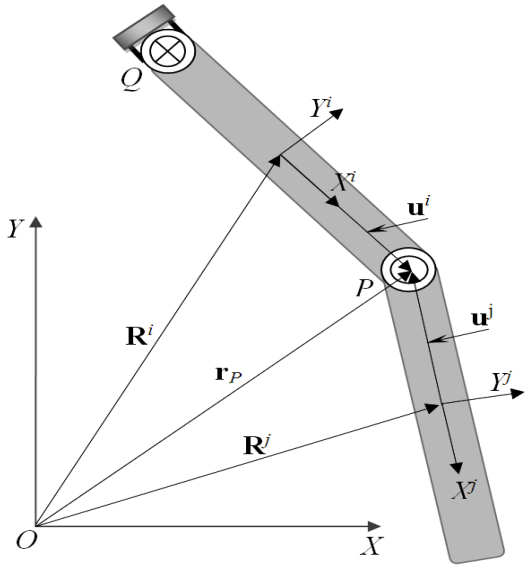

Figure 3 Double pendulum example

In this simple planar rigid body example, the kinematic constraint conditions of the pin joint can be written as $\mathbf{r}_P^i = \mathbf{r}_P^j$. This equation can be written more explicitly in terms of the co-ordinates of bodies i and j, as

$$\mathbf{R}^i + \mathbf{A}^i \bar{\mathbf{u}}_P^i = \mathbf{R}^j + \mathbf{A}^j \bar{\mathbf{u}}_P^j \tag{1}$$

where $\mathbf{R}^i$ and $\mathbf{R}^j$ define the global position vector of the origins of the coordinates systems of the two bodies, and $\mathbf{A}^i$ and $\mathbf{A}^j$ are the transformation matrices that define the orientations of the two bodies. In the planar analysis, the vectors and matrices that appear in Eq. 1 can be written as

$$\left.\begin{aligned} \bar{\mathbf{u}}_P^k &= [\bar{x}^k \quad \bar{y}^k], \qquad \mathbf{R}^k = [R_x^k \quad R_y^k] \\ \mathbf{A}^k &= \begin{bmatrix} \cos(\theta^k) & -\sin(\theta^k) \\ \sin(\theta^k) & \cos(\theta^k) \end{bmatrix}, \quad k = i, j \end{aligned}\right\} \tag{2}$$

The geometric nonlinearities of the connectivity condition of Eq.1 characterize all MBS formulations including the augmented and embedding techniques. Using the embedding technique, one can show that the two equations of motion of the planar rigid body double pendulum shown in Fig. 3 can be written as

$$\left.\begin{aligned}
&\left(m^i (l^i)^2 + J^i + m^j (l^i)^2\right)\ddot{\theta}^i + \left(2m^j l^i l^j \cos\theta^{ij}\right)\ddot{\theta}^j = \\
&\qquad -2m^i g l^i \cos\theta^i - m^j g l^i \cos\theta^i - 2m^j l^i l^j \left(\dot{\theta}^j\right)^2 \sin\theta^{ij} \\
&\left(2m^j l^i l^j \cos\theta^{ij}\right)\ddot{\theta}^i + \left(m^j (l^j)^2 + J^j\right)\ddot{\theta}^j = \\
&\qquad -2m^j g l^j \cos\theta^j + m^j l^i l^j \left(\dot{\theta}^i\right)^2 \sin\theta^{ij}
\end{aligned}\right\} \tag{3}$$

In this equation, m^k and l^k are, respectively, the mass and length of link $k, k = i, j$, $\ddot{\theta}^k$ is the angular acceleration of link k, $\theta^{ij} = \theta^i - \theta^j$ and g is the gravity constant. It is clear from Eq. 3 that the equations of motion for a simple planar rigid body double pendulum are highly nonlinear as the result of the nonlinear connectivity conditions. The resulting inertia coefficients are also highly nonlinear because of the geometric nonlinearities that result from the non-structural discontinuities. Such non-structural geometric discontinuities also lead to more geometric nonlinearities when the deformation of the links are considered using the FE/FFR formulation due to the dynamic coupling between the reference motion and the elastic deformations. In the FFR formulation, $\bar{\mathbf{u}}_P^k$ is expressed in terms of the elastic coordinates and the number of equations of motion increases by the number of these elastic coordinates.

3 B-SPLINE CURVES AND SURFACES

In B-spline representation, any curve can be represented as a combination of several polynomial segments. Generally, B-spline curves can be defined using following equation [1, 18]:

$$\mathbf{r}(u) = N_{0,p}(u)\mathbf{P}_0 + N_{1,p}(u)\mathbf{P}_1 + \ldots\ldots + N_{n,p}(u)\mathbf{P}_n = \sum_{i=0}^{n} N_{i,p}(u)\mathbf{P}_i \tag{4}$$

where $N_{i,p}(u)$ are the B-spline basis functions of degree p, u is the parameter, and $\mathbf{P}_i$ are the control points that define the control polygon. The basis functions can be defined as

$$\left.\begin{aligned}
N_{i,0}(u) &= \begin{cases} 1 & \text{if } u_i \le u < u_{i+1} \\ 0 & \text{otherwise} \end{cases} \\
N_{i,j}(u) &= \frac{u - u_i}{u_{i+j} - u_i} N_{i,j-1}(u) + \frac{u_{i+j+1} - u}{u_{i+j+1} - u_{i+1}} N_{i+1,j-1}(u)
\end{aligned}\right\} \tag{5}$$

where $u_i \le u_{i+1}$, and U= $\{u_0\ u_1 \ldots . u_{n+p+1}\}$ is called the knot vector. The elements of the knot vector need not be distinct. Each nonzero span corresponds to a B-spline segment defined by two knot points called in this case breakpoints that represent distinct knot values. The number of equal knots at a point is referred to as the knot multiplicity.

B-spline surfaces can also be defined using the product of B-spline base functions, two parameters, and two knot vectors. B-spline surfaces can be defined in the following parametric form [1, 18]:

$$\mathbf{r}(u,v)=\sum_{i=0}^{n}\sum_{j=0}^{m}N_{i,p}(u)N_{j,q}(v)\mathbf{P}_{i,j} \tag{6}$$

where u and v are the parameters; $N_{i,p}(u)$ and $N_{j,q}(v)$ are B-spline basis functions of degree p and q, respectively; and $\mathbf{P}_{i,j}$ are a set of bidirectional net of control points. $N_{j,q}(v)$ can be defined similar to the definition introduced for $N_{i,p}(u)$ with another knot vector $\mathbf{V}=\{v_0 \quad v_1 \quad \cdots \quad v_{m+q+1}\}$. Note that the orders of the polynomials in the u and v directions can be different; for example, a cubic interpolation can be used along u while a linear interpolation can be used along v. As in the case of B-spline curves, the knots of B-spline surfaces do not have to be distinct; distinct knots are called breakpoints and define surface segments with non-zero dimensions. The number of the non-distinct knots in $\mathbf{U}$ and $\mathbf{V}$ at a point is referred to as the knot multiplicity associated, respectively, with the parameters u and v at this point. At a given breakpoint, the multiplicity associated with u can be different from the multiplicity associated with v; allowing for different degrees of continuity for the derivatives with respect to u and v. For cubic $N_{i,p}$ ($p=3$), C^0, C^1, or C^2 conditions correspond, respectively, to knot multiplicity of three, two, and one; while in the case of linear interpolation of $N_{j,q}$, the highest continuity degree that can be demanded is continuity of the gradients.

In B-spline surface representation, there is a relationship between the polynomial degree, the number of knots, and the number of control points. This relationship must be fully understood if B-spline geometry will be used as an analysis tool. If $r+1$ is the number of knots in $\mathbf{U}$ and $s+1$ is the number of knots in $\mathbf{V}$, then in B-spline geometry, one must have

$$r=n+p+1, \quad s=m+q+1 \tag{7}$$

These formulas imply that, for a given polynomial order, if the number of knots decreases, the number of control points (degrees of freedom used in the analysis) must also decrease. A decrease in the knot multiplicity by one is equivalent to eliminating one control point. This can also be equivalent to increasing the degree of continuity since eliminating a control point can be the result of imposing algebraic equations that relates the derivatives at a certain breakpoint. From the bidirectional structure used in Eq. 6, a surface segment which has cubic interpolation along u ($p=3, n=3, r+1=8$) and a linear interpolation along v ($q=1, m=1, s+1=4$), should have $(n+1)\times(m+1)=8$ control points; this is regardless of whether the surface is two- or three-dimensional. Manipulation of the B-spline surface of Eq.6 shows that these eight control points are the result of using the alternate basis set $1, u, v, uv, u^2, u^2v, u^3, u^3v$. That is, B-spline representation and the formulas of Eq. 7 do not allow for the use of the basis set $1, u, v, uv, u^2, u^3$ which can be effectively used to develop a shear deformable beam model. If a cubic interpolation is used for both u and v (thin plate), the B-spline representation will require 16 control points because the expansion must include all terms $u^k v^l$; $k,l=0,1,2,3$ regardless of whether the shape of deformation of the plate is simple or complex; one must strictly follow the B-spline rigid structure. This can be of disad-

vantage in the analysis since such a geometric representation can unnecessarily increase the dimension of the analysis model and leads to the loss of the flexibility offered by the FE method or modal analysis techniques. As the degree of the polynomial interpolation increases, the problem gets even worse.

4 ANCF FINITE ELEMENT GEOMETRY

In the absolute nodal coordinate formulation, the position vector of any arbitrary point of the finite element with respect to the fixed global reference frame can be generally written as follows

$$\mathbf{r}(x,y)=\mathbf{S}(x,y)\mathbf{e}(t) \tag{8}$$

where x and y are the element spatial coordinates, t is time, $\mathbf{S}$ is the element shape function matrix, and $\mathbf{e}$ is the vector of the element nodal coordinates. An example of ANCF elements can be planar two-node shear deformable beam element. The shape function matrix for this element is defined as

$$\mathbf{S}=\begin{bmatrix} s_1\mathbf{I} & s_2\mathbf{I} & s_3\mathbf{I} & s_4\mathbf{I} & s_5\mathbf{I} & s_6\mathbf{I} \end{bmatrix} \tag{9}$$

In this equation, $\mathbf{I}$ is the identity matrix, and $s_i, i=1,2,\ldots,6$ are shape functions defined as [16]:

$$\left.\begin{aligned} &s_1=1-3\xi^2+2\xi^3, \quad s_2=l\left(\xi-2\xi^2+\xi^3\right), \quad s_3=l\eta\left(1-\xi\right),\\ &s_4=3\xi^2-2\xi^3, \quad s_5=l\left(-\xi^2+\xi^3\right), \quad s_6=l\xi\eta \end{aligned}\right\} \tag{10}$$

where l is the element length, $\xi=\dfrac{x}{l}$ and $\eta=\dfrac{y}{l}$.

Each of the element nodes has six degrees of freedom; two translational coordinates defined by the two-dimensional vector $\mathbf{r}=\begin{bmatrix} r_1 & r_2 \end{bmatrix}^{\mathbf{T}}$, and four gradient coordinates defined by the two vectors $\mathbf{r}_x=\begin{bmatrix} r_{x1} & r_{x2} \end{bmatrix}^{\mathbf{T}}$ and $\mathbf{r}_y=\begin{bmatrix} r_{y1} & r_{y2} \end{bmatrix}^{\mathrm{T}}$. The vector of nodal coordinates $\mathbf{e}$ can then be written as

$$\mathbf{e}=\begin{bmatrix} \mathbf{r}^{A\mathrm{T}} & \mathbf{r}_x^{A\mathrm{T}} & \mathbf{r}_y^{A\mathrm{T}} & \mathbf{r}^{B\mathrm{T}} & \mathbf{r}_x^{B\mathrm{T}} & \mathbf{r}_y^{B\mathrm{T}} \end{bmatrix}^{\mathrm{T}} \tag{11}$$

In this equation, A and B refer to the end points of the finite element. Note that the element defined by the preceding equations is based on a cubic interpolation for x and a linear interpolation for y. This element has been widely used in the analysis of large deformation problems. The standard ANCF assembly process ensures continuity of both position and gradient coordinates when two finite elements are rigidly connected.

Structural discontinuities can be systematically modeled using ANCF finite elements by using the proper gradient transformations. The gradient transformations, which are different from vector transformations, enter into the formulation of the element dynamic equations. Furthermore, constraints on higher derivatives can also be imposed at a preprocessing stage using linear algebraic equations; allowing for having a higher degree of continuity.

5 ANCF VS B-SPLINE CURVES AS ANALYSIS TOOLS

While B-spline geometry can always be converted to ANCF geometry, the converse is not true. ANCF geometry does not impose restriction on the basis functions that must be included in the interpolating polynomials. This allows for developing finite elements that have less coordinates as compared to those developed using the B-spline representation. Furthermore, ANCF geometry can be used to model both structural and non-structural discontinuities [13, 15, 17, and 18], while the rigid recurrence formula for B-spline representation cannot be used to model structural discontinuities in a straight forward manner. The basic differences between ANCF and B-spline geometries are demonstrated in this section using a planar beam example. This element is an example of ANCF elements that cannot be converted to B-spline representation. This element is based on a polynomial expansion that does not have the two basis functions x^2y and x^3y. These terms can be included in ANCF geometry by adding nodal coordinates allowing for converting B-spline representation to ANCF representation. Similar comments apply to ANCF thin plate elements that do not have to include all the basis functions $x^k y^l; k,l = 0,1,2,3$. This flexibility offered by ANCF geometry allows for developing finite elements that have smaller number of coordinates compared to those elements developed by B-spline geometry.

One can also show that ANCF finite elements can describe structural and non-structural discontinuities. Non-structural discontinuities that allow for large rigid body rotations can be described using a C^0 model obtained by imposing constraints on the position coordinates only. For example if two elements i and j are connected by pin joint at a node, one can apply the algebraic equations $\mathbf{r}^i = \mathbf{r}^j$ at this node. These algebraic equations can be imposed at a preprocessing stage to eliminate the dependent variables and define FE mesh that has a constant mass matrix and zero Coriolis and centrifugal forces despite the finite rotations allowed between the finite elements of the mesh. Non-structural discontinuities can also be described using B-spline geometry by reducing the knot multiplicity at the joint node by one. Note that in the case of non-structural discontinuities no constraints are imposed on the gradient vectors, and therefore, the state of strain is not unique at the joint node. Each of the Lagrangian strains $\varepsilon_{xx} = \left(\mathbf{r}_x^T\mathbf{r}_x - 1\right)/2$, $\varepsilon_{yy} = \left(\mathbf{r}_y^T\mathbf{r}_y - 1\right)/2$, and $\varepsilon_{xy} = \mathbf{r}_x^T\mathbf{r}_y/2$ have two values at the joint node; one defined on element i and the other is defined on element j. Here $\mathbf{r}_x = \partial\mathbf{r}/\partial x$, $\mathbf{r}_y = \partial\mathbf{r}/\partial y$, $\mathbf{r}_z = \partial\mathbf{r}/\partial z$.

The concept of degrees of freedom widely used in mechanics is not considered in developing the recurrence relationships on which B-spline and NURBS geometry are based. This represents another serious limitation when these computational geometry methods are used as analysis tools; as evident by the fact that B-spline geometry cannot describe structural discontinuities. This type of discontinuities, while it remains of the C^0 continuity type, requires imposing additional constraints on the gradients; these constraints cannot be captured by the B-spline recurrence formula since they require the elimination of additional vectors. In the case of B-spline, C^0 continuity is achieved by reducing the knot multiplicity by one, and this eliminates one control point leading to the definition of a pin joint (non-structural discontinuity). ANCF geometry, on the other hand, allows for imposing constraints on the gradients using the tensor transformation $\left(\partial\mathbf{r}/\partial\mathbf{x}_1\right) = \left(\partial\mathbf{r}/\partial\mathbf{x}_2\right)\mathbf{A}$, where $\mathbf{x}_1 = \begin{bmatrix} x_1 & y_1 \end{bmatrix}^T$ and $\mathbf{x}_2 = \begin{bmatrix} x_2 & y_2 \end{bmatrix}^T$ are two sets of coordinate lines, and $\mathbf{A}$ is the matrix of coordinate line transformation. Using this tensor gradient transformation, the structural discontinuities can be systematically modeled using ANCF finite elements [13, 17].

6 NEW ANCF FINITE ELEMENT MESH

In this section, it is shown how fully parameterized ANCF three-dimensional finite elements can be used to develop spatial joint models that allow large relative rigid body rotation between the finite elements. ANCF finite elements connected by this joint can be assembled using linear connectivity conditions leading to FE mesh that has a constant mass matrix and zero Coriolis and centrifugal forces. The fully parameterized three-dimensional ANCF beam element is used in this investigation to demonstrate the development of such joint models. The displacement field of the element can be written as $\mathbf{r}(x, y, z) = \mathbf{S}(x, y, z)\mathbf{e}(t)$ where x, y, and z are the element spatial coordinates [12, 19]. The element has two nodes; each node has 12 nodal coordinates defined by the vector $\mathbf{e}^k = \left[\mathbf{r}^{kT} \quad \mathbf{r}_x^{kT} \quad \mathbf{r}_y^{kT} \quad \mathbf{r}_z^{kT}\right]^T$, where k is the node number. This ANCF finite element captures the cross section deformation and its coupling with extension and bending. Therefore, this element can be used to develop general models for belt drives and rubber tracked vehicles. Furthermore, this three-dimensional beam element is another example that can be used to demonstrate the generality of the ANCF geometry. This element is based on cubic interpolation in x and linear interpolation in y and z. Nonetheless, one can show that the four basis functions x^2y, x^3y, x^2z, x^3z are not used in developing the displacement field of this widely used ANCF beam element. Therefore, the geometry of this element cannot be converted to B-spline volume geometry. These missing basis functions can be systematically included in the development of another ANCF finite element that can be converted to B-spline volume geometry. However, such an element will lead to 50% increase in the number of the element nodal coordinates.

A planar pin joint between rigid or flexible bodies is an example of C^0 continuity, as previously discussed. A pin joint between two rigid bodies in the spatial analysis also allows for only one degree of freedom, which is a relative rotation about the joint axis. Since the pin joint eliminates five degrees of freedom in the rigid body analysis, its formulation requires five algebraic constraint equations that eliminate three relative translation displacements and two relative rotations between the two bodies. In the case of flexible bodies, an infinitesimal volume can have 12 modes of displacements; three rigid body translations, three rotations, and six deformation modes. In this section, a new model of pin joint between ANCF finite elements is introduced. The formulation of this pin joint between elements i and j employs the following six scalar equations defined at the joint node:

$$\mathbf{r}^i = \mathbf{r}^j, \qquad \mathbf{r}_\alpha^i = \mathbf{r}_\alpha^j \tag{12}$$

Here α is the coordinate line that defines the joint axis; α can be x, y, z or any other coordinate line as discussed later in this section. The six scalar equations of Eq. 12 eliminate six degrees of freedom; three translations, two rotations, and one deformation mode. This joint model ensures C^1 continuity with respect to the coordinate line α and C^0 continuity with respect to the other two parameters. It follows that the Lagrangian strain component $\varepsilon_{\alpha\alpha} = \left(\mathbf{r}_\alpha^T\mathbf{r}_\alpha - 1\right)/2$ is continuous at the joint definition point, while the other five strain components can be discontinuous.

While the algebraic constraint equations of a pin joint between two rigid bodies are highly nonlinear. The algebraic constraint equations of Eq. 12 are linear. Therefore, these equations

can be applied at a preprocessing stage to systematically eliminate the dependent variables. Using these equations, one can develop a new kinematically linear FE mesh for flexible-link chains in which the links can have arbitrarily large relative rotations. The use of this pin joint model with ANCF finite elements leads to a constant mass matrix and zero Coriolis and centrifugal forces.

As previously mentioned in this paper, B-spline geometry can describe the type of non-structural discontinuity discussed in this section. Nonetheless, if an arbitrary axis of a pin joint is to be used in the analysis, the use of B-spline geometry can be difficult given the rigid structure of the B-spline recurrence formula. In order to be able to choose an arbitrary axis of rotation for the pin joint, one must be able to define the gradient vector in the direction of a coordinate line along this axis of rotation. Such a definition can be easily made using ANCF geometry using the gradient tensor transformation. Let u, v, and w be another set of parameters; one of them can be used to define the joint axis. It follows that $\left[\mathbf{r}_u \quad \mathbf{r}_v \quad \mathbf{r}_w\right] = \left[\mathbf{r}_x \quad \mathbf{r}_y \quad \mathbf{r}_z\right]\mathbf{A}$, where $\mathbf{A}$ is the constant matrix of coordinate transformation defined as

$$\mathbf{A} = \begin{bmatrix} \dfrac{\partial x}{\partial u} & \dfrac{\partial x}{\partial v} & \dfrac{\partial x}{\partial w} \\ \dfrac{\partial y}{\partial u} & \dfrac{\partial y}{\partial v} & \dfrac{\partial y}{\partial w} \\ \dfrac{\partial z}{\partial u} & \dfrac{\partial z}{\partial v} & \dfrac{\partial z}{\partial w} \end{bmatrix} \tag{13}$$

The fact that this matrix is constant allows having linear pin joint connectivity conditions when ANCF finite elements are used [13, 17].

7 NUMERICAL RESULTS

It will be demonstrated in this section that ANCF meshes that allow relative motion between the finite elements can be developed. In these ANCF meshes, the finite elements are connected using linear algebraic equations and the mesh mass matrix remains constant. Chain example characterized by non-structural discontinuities is considered in this section. The links of the chain used in this section are assumed to be flexible with mass density of 7200 kg/m^3, and a Poisson ratio of 0.3. Two different values of the modulus of elasticity, 2×10^8 and 2×10^{11} N/m^2, are used in the simulations. The elastic forces of the ANCF elements are formulated using a general continuum mechanics approach that employs a Hookean constitutive model. The system is represented by one FE mesh (one flexible body).

The chain used is a multi-link chain that has an overall length of 1 m (Fig. 2). It consists of 8 links that are connected by pin joints. These pin joints ensure C^0 continuity and allow for independent relative rotations and deformation modes at the joint nodes. In computational geometry, this case of non-structural discontinuities at the joint nodes corresponds to knot multiplicity of 3 when cubic polynomials are used for the finite elements. Each link in this chain is represented by one planar shear deformable beam element. Therefore, the chain has 80 degrees of freedom; 8 degrees of freedom represent rigid body relative rotations, and the remaining 72 degrees of freedom represent deformation modes; with 9 deformation modes for each link. The chain is subjected to a base excitation defined by the func-

tion $X = -0.01\sin(0.1\pi\, t)$. All the links of the chain are assumed to be initially horizontal. The effect of the link gravity is considered.

In order to verify the obtained results, a simulation of a very stiff pendulum is carried out first, and the results are compared with the results of a rigid link chain model. For the very stiff chain, a modulus of elasticity of $2\times10^{11}\,\mathrm{N/m^2}$ is used for the finite elements. Figure 4 shows the vertical position of the center of the last link as function of time for both cases of the rigid and stiff chains.

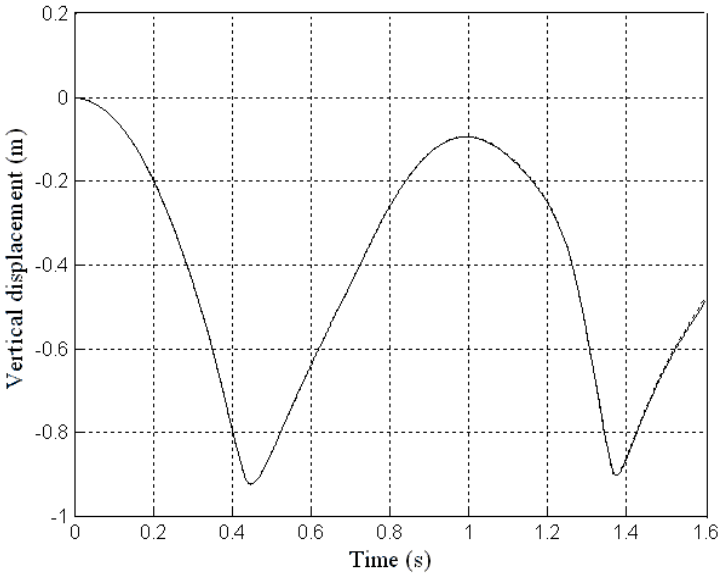

Figure 4 Vertical displacement of the center of link 8

(—— Flexible link chain, ---- Rigid link chain)

Figure 5 shows the absolute rotation of the last link of the chain about an axis parallel to the pin join axes. The results presented in Figs. 4 and 5 show a good agreement between the results obtained using the rigid and very stiff link chain models. For the rigid link chain model, nonlinear algebraic equations are used to define the pin joints and the resulting generalized mass matrix associated with the system degrees of freedom is highly nonlinear. For the flexible ANCF chain model, the chain is represented by one FE mesh (one flexible body), the pin joint constraints are linear, and the mass matrix is constant. Figure 6 shows the vertical displacement of the tip point of link 8 of the chain when the modulus of elasticity is reduced to $2\times10^{8}\,\mathrm{N/m^2}$. Figure 7 shows the relative rotation between links 7 and 8 of the flexible chain as function of time.

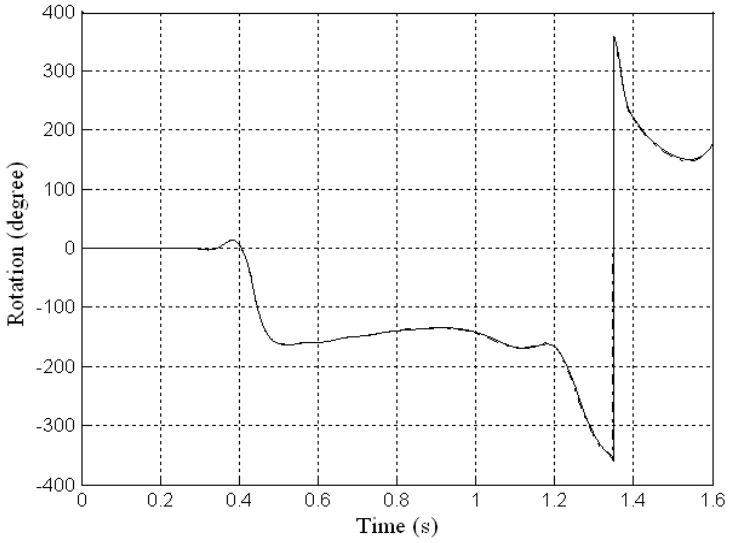

Figure 5 Rotation of link 8 (—— Flexible link chain, ---- Rigid link chain)

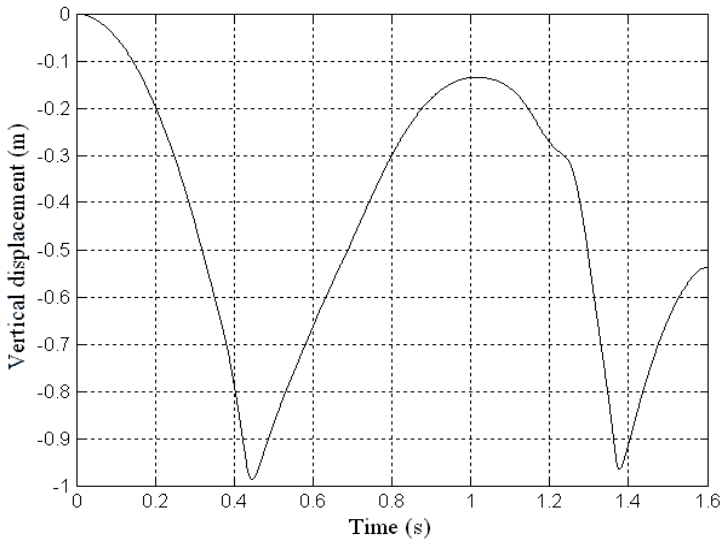

Figure 6 Vertical displacement of the tip point of link 8 of the flexible chain

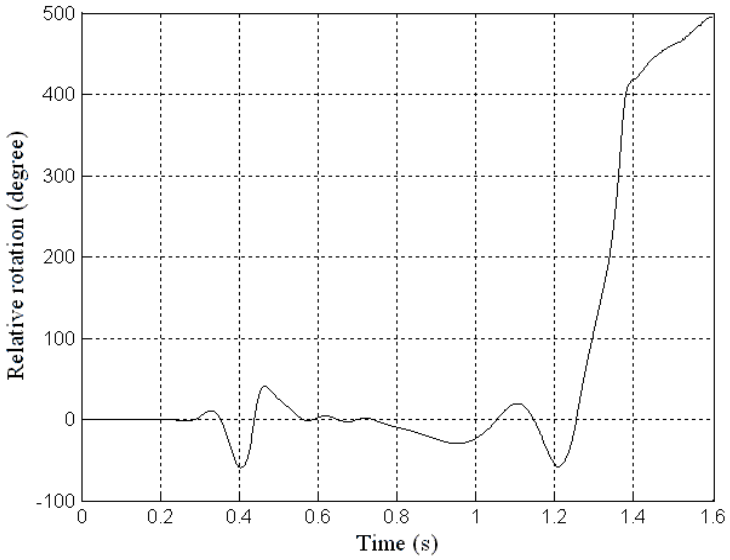

Figure 7 Relative rotation between last two chain links

Figures 8 and 9 show the distribution of the normal strain components ε_{xx} and ε_{yy}. It is clear from the results presented in these figures that the strains are discontinuous as the result of the non-structural discontinuities at the joints; the strains are continuous within the elements, and ε_{xx} decreases since the links at the beginning of the chain are subjected to higher gravity forces as compared to the links at the end of the chain. It is important, however, to point out that for fully parameterized ANCF finite elements one can always define at an arbitrary point inside the element, coordinate lines in which there are continuous strain components regardless of the shape of the structure.

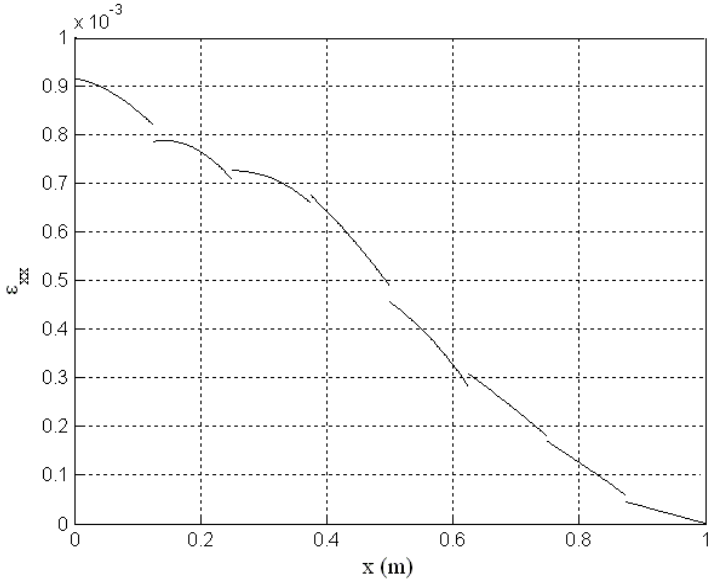

Figure 8 Distribution of the normal strain ε_{xx}

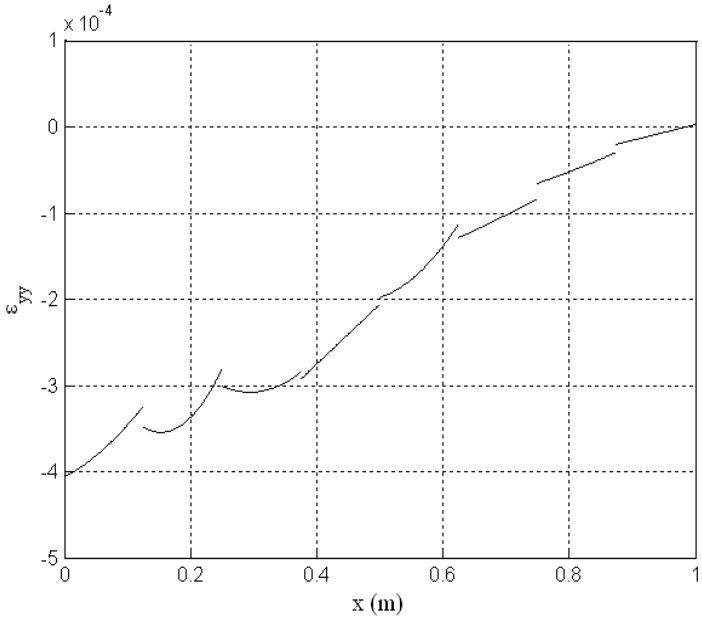

Figure 9 Distribution of the normal strain ε_{yy}

8 CONCLUSIONS

This paper addresses the important issue of using computational geometry methods such as B-spline and NURBS as analysis tools. B-spline and NURBS employ recurrence formulas that allow changing the degree of continuity at a breakpoint by adjusting the knot multiplicity at this point. As demonstrated in this paper, the recurrence formula has several drawbacks when B-spline representation is used as an analysis tool. Because the recurrence formula does not provide flexibility for choosing the basis functions, B-spline representation can lead to significantly larger number of coordinates and a higher dimensional model. This fact was used to demonstrate the generality of the ANCF geometry. While B-spline geometry can always be converted to ANCF geometry, the converse is not true. It is also shown that the B-spline recurrence formula cannot be used to model structural discontinuity in a straight forward manner. While structural discontinuities are of the C^0 type, they cannot be captured in the B-spline representation by reducing the knot multiplicity by one. This reduction of the knot multiplicity is equivalent to elimination of the relative translation only; and such a reduction in the knot multiplicity leads to a rigid body mode that defines the conditions of a pin joint. In the case of structural discontinuities, on the other hand, the C^0 B-spline representation does not eliminate the rigid body mode since additional algebraic constraint equations are required in order to eliminate the relative rotations between two segments. The paper also presents a new three-dimensional pin joint model that leads to linear connectivity conditions and constant mass matrix when used with ANCF finite elements. The limitations identified in this paper when B-spline geometry is used as analysis tool suggest the use of the I-CAD-A approach in which a constant transformation can be developed to convert CAD geometry to FE mesh.

REFERENCES

[1] L. Piegl, W. Tiller, *The NURBS Book*. 2nd edn. Springer, New York, 1997.

[2] G.G. Sanborn, A.A. Shabana, On The Integration of Computer Aided Design and Analysis Using The Finite Element Absolute Nodal Coordinate Formulation. *Multibody System Dynamics*, Vol. 22, pp. 181–197, 2009.

[3] P. Lan, A.A. Shabana, Integration of B-spline Geometry and ANCF Finite Element Analysis. *Nonlinear Dynamics*, DOI 10.1007/s11071-009-9641-6, 2010.

[4] O. N. Dmitrochenko, D.Y. Pogorelov, Generalization of Plate Finite Elements for Absolute Nodal Coordinate Formulatio. *Multibody System Dynamics*, Vol. 10, no. 1: 17-43, 2003.

[5] K.E. Dufva, J.T. Sopanen, A.M. Mikkola, A Two-Dimensional Shear Deformable Beam Element Based on the Absolute Nodal Coordinate Formulation. *Sound and Vibration*, Vol. 280, pp. 719-738, 2005.

[6] D. Garcia-Vallejo, J. Mayo, J. L. Escalona, Three-Dimensional Formulation of Rigid-Flexible Multibody Systems with Flexible Beam Elements. *Multibody System Dynamics*, Vol. 20 (1), pp. 1-28, 2008.

[7] K.S. Kerkkänen, D. García-Vallejo, A.M. Mikkola, Modeling of Belt-Drives using a Large Deformation Finite Element Formulation. *Nonlinear Dynamics*, Vol.43, pp. 239-256, 2006.

[8] A.L. Schwab, J.P .Meijaard, Comparison of Three-Dimensional Flexible Beam Elements for Dynamic Analysis: Classical Finite Element Formulation and Absolute Nodal Coordinate Formulation. *Journal of Computational and Nonlinear Dynamics*, Vol. 5 (1), 011010-1 – 011010-10, 2010.

[9] Q. Tian, L.P. Chen, Y.Q. Zhang, J.Z. Yang, An Efficient Hybrid Method for Multibody Dynamics Simulation Based on Absolute Nodal Coordinate Formulation. *ASME Journal of Computational and Nonlinear Dynamics*, Vol. 4, pp. 021009-1 - 021009-14 , 2009.

[10] Q. Tian, Y. Zhang, L. Chen, J. Yang, Simulation of Planar Flexible Multibody Systems with Clearance and Lubricated Revolute Joints. *Nonlinear Dynamics*, Vol. 60, pp. 489-511, 2010.

[11] W.S. Yoo, J.H. Lee, S.J. Park, J.H. Sohn, D.Pogorelov, O. Dimitrochenko, Large Deflection Analysis of a Thin Plate: Computer Simulation and Experiment. *Multibody System Dynamics*, Vol. 11, pp. 185-208, 2004.

[12] R.Y. Yakoub, A.A. Shabana, Three Dimensional Absolute Nodal Coordinate Formulation for Beam Elements: Implementation and Application. *ASME Journal for Mechanical Design*, Vol. 123, pp. 614–621, 2001.

[13] A.A. Shabana, A.M. Mikkola, Use of the Finite Element Absolute Nodal Coordinate Formulation in Modeling Slope Discontinuity. *ASME Journal for* Mechanical *Design*, Vol. 125(2), pp. 342–350, 2003.

[14] L.K. Abbas, X. Rui, Z.S. Hammoudi, Plate/Shell Element of Variable Thickness Based on the Absolute Nodal Coordinate Formulation. *IMechE Journal of Multibody Dynamics*, Vol. 224, Part K, pp. 127-141, 2010.

[15] A.M. Hamed, A.A. Shabana, P. Jayakumar, M.D. Letherwood, Non-Structural Geometric Discontinuities in Finite Element/Multibody System Analysis. *Nonlinear Dynamics*, 2011, in press.

[16] M.A. Omar, A.A. Shabana, A Two-Dimensional Shear Deformation Beam for Large Rotation and Deformation. *Journal of Sound and Vibration*, Vol. 243(3), pp. 565–576, 2001.

[17] A.A. Shabana, General Method for Modeling Slope Discontinuities and T-Sections using ANCF Gradient Deficient Finite Elements. *ASME Journal of Computational and Nonlinear Dynamics*, 2010, in press.

[18] A.A. Shabana, A.M. Hamed, A.A Mohamed, P. Jayakumar, M.D. Letherwood, Development of New Three-Dimensional Flexible-Link Chain Model Using ANCF Geometry. Technical Report # MBS2011-1-UIC, Department of Mechanical Engineering, University of Illinois at Chicago, Chicago, 2011.

[19] A.A. Shabana, *Computational Continuum Mechanics*. Cambridge University Press, Cambridge, 2008.